

Despeckling of SAR Images Using Intensity Coherence Vector

¹D. Suresh and ²P. Alli

¹PSNA College of Engineering and Technology, Dindigul, Tamil Nadu, India

²Velammal College of Engineering and Technology, Madurai, Tamil Nadu, India

Abstract: Noise will be unavoidable in image acquisition practice and denoising is a necessary step to recover the image quality. Synthetic Aperture Radar (SAR) images are inherently exaggerated by speckle noise which occurs due to coherent nature of the scattering phenomena. Denoising SAR images aim at removing speckle while preserving image features such as texture, edges and point targets. The mixture of nonlocal grouping and transformed domain filtering has directed the modern denoising techniques. However, this approach makes a tough assumption that image patch itself provides an excellent approximation on the true parameter which leads to bias problem predominantly under serious speckle noise. Another disadvantage is that the generally used patch pre-selection methods cannot efficiently exclude the outliers and damage the edges. In this study, the SAR image is injected with speckle noise and then edge based marker controlled watershed segmentation is applied to identify the homogeneous regions in SAR image. For each region, the neighborhood pixels are identified by using Intensity Coherence Vector (ICV) and are denoised independently by using a local mean filtering. By separating coherent pixels from incoherent pixels, ICV's provide finer distinctions among blocks; finally, the blocks are aggregated to form the denoised image. The experimental results show that the proposed method outperforms other methods such as patch-based filtering, non-local means, wavelets and classical speckle filters in terms higher signal-to-noise and edge preservation ratios comparatively.

Key words: SAR image, speckle noise, coherence vector, watershed, edge

INTRODUCTION

Synthetic Aperture Radar (SAR) imaging is used in various applications such as urban planning, cartography, land cover mapping and cartography. The SAR imaging systems are very useful of acquiring information in different climatic conditions. Naturally, SAR images are disturbed from speckle noise which degrades the performance of automatic SAR image interpretation and analysis. Hence, the SAR image analysis system starts with a preprocessing step to remove the speckle noises before preceding the major steps like segmentation and classification (Ren *et al.*, 2011; Chen *et al.*, 2012; Li *et al.*, 2012). But at the same time, the despeckling step should not disturb the other image features such as shapes, boundaries and textures.

Numerous filtering algorithms have been proposed in the last several decades for SAR images speckle denoising (Lee *et al.*, 1994), most of which are based on the statistics of pixels and their relationship with their surroundings (Lee, 1981; Deledalle *et al.*, 2009; Parrilli *et al.*, 2012). In addition, pixels even in one image can follow dissimilar statistical scatterings which bring

complications in estimating parameters (Cheng *et al.*, 2013). In contrast, Liu *et al.* (2013) introduced an alternative way for despeckling which suppresses speckle without modeling the speckle directly. The despeckling algorithms can be classified into two categories: the first category takes L different looks of SAR images of the same scene and average them to reduce speckle noise. However, it also reduces ground resolution of the image in proportion to the number of looks. The second category of approaches works with single image of a scene with speckle filtering algorithms both in spatial and frequency domain (Molina *et al.*, 2012; Iqbal *et al.*, 2013). This study focuses on the first category. The classical filters (Lee, 1980, 1986; Frost *et al.*, 1982; Kuan *et al.*, 1985; Lee *et al.*, 1994) can be used to denoise SAR images in spatial domain. These filters work by dividing the SAR images into sub-windows and for each sub-window the center pixel is replaced based on the uniformity of the pixels available in the sub-window. These approaches can produce better denoising in static images. In case of SAR images, they either preserve speckle noise or damage the weak signals at heterogeneous areas such as edge, point targets or texture area.

The gamma-MAP filter (Lopez *et al.*, 1990) and the refined gamma-MAP filter (Baraldi and Parmiggiani, 1995) later consider both the speckle model and the reflectivity probability density functions. The gamma-MAP filter highly depends on the description of the gamma value. However, the choices of local window size and orientation have greater impact on the performance of these spatial filters. Most of these filters use a local analysis window with fixed size and shape, although adjustable windows of these algorithms for local spatial variations are required. Yu and Acton (2002) proposed a Speckle Reduction Anisotropic Diffusion (SRAD) filter to despeckle the SAR images as well as to preserve image edges better.

From the literature, it is noted that, denoising in transformed domain has been more efficient than in spatial domain. The advantage is that the noise and the signal can be easily separated in transformed domain rather than spatial domain. The wavelet techniques are the most popular transform techniques used in the field of denoising which decomposes the images into four different components where the high-frequency components are considered as noisy area and they are denoised by filtering the wavelet coefficients. This idea has proved great success to denoise Additive White Gaussian Noise (AWGN). Gagnon and Jouan in 1997 presented a comparative study between a wavelet filter and several classical speckle filters that are widely used in SAR image denoising. The study shows that the wavelet-based filter is among the best speckle filters, which performs equally well for low-level speckle noise and it slightly outperforms for higher-level speckle noise. A robust threshold estimator is still needed in order to automate the filtering process. Several denoising algorithms have been proposed in the literature by using wavelet based filtering for despeckling SAR images (Foucher *et al.*, 2001; Argenti and Alparone, 2002; Achim *et al.*, 2003; Sveinsson and Benediktsson, 2003; Gleich and Datcu, 2007; Ranjani and Thiruvengadam, 2010). These methods smoothened the homogeneous areas while preserving strong scatterers and edges. However, they do not work well in the heterogeneous areas: the edges and textures are still blurred in some degrees. Additionally, they often suffered from computational cost. A large number of studies have been developed to address these problems (Xie *et al.*, 2002; Pizurica *et al.*, 2003; Zhou and Shui, 2007; Easley *et al.*, 2008; Hou *et al.*, 2012). However, since the performance of denoising is very sensitive to logarithmic operation that tends to distort the radiometric properties of the SAR image, techniques based on Additive Signal-Dependent

Noise (ASDN) model were developed in Bianchi *et al.* (2008). Recently, Lu *et al.* (2013) proposed a new SAR image despeckling method by using multiscale products based on directionlets. They multiplied the adjacent scale subbands to amplify significant features and then applied the threshold to multiscale products instead of the single-scale directionlet coefficients directly. The experimental results on test SAR image showed that the proposed method reduces speckle effectively while preserving edge structures. However, these wavelet based methods also have the following three main shortcomings: the multilevel transform cannot identify the edges and contours accurately, the down sampling in wavelet transform is time-variant (Dai *et al.*, 2004) and thresholding the wavelet coefficients cannot detect the edges from noise efficiently.

Some of the existing methods based on Principal Component Analysis (PCA) have shown better performance, as PCA has adequate ability to represent the structural features such as texture and boundaries. Muresan and Parks (2003) proposed an adaptive PCA denoising approach and Zhang *et al.* (2010) proposed a Local Pixel Grouping PCA (LPG-PCA). These are the recent examples for PCA based denoising schemes. Xu *et al.* (2014) presented an SAR image denoising scheme based on clustering noisy image into disjoint local regions and denoising each region by using LMMSE filtering in PCA domain. All these methods have outperformed the conventional wavelet-based denoising methods. But still, the PCA based denoising is not much adopted for SAR images.

Another method of SAR image denoising, Non-Local Means (NLM) is initiated (Buades *et al.*, 2005) where the pixels with homogeneous spatial structure is considered even at "nonlocal" pixels, rather than denoising with local pixels. For instance, the Probabilistic Patch-Based (PPB) filter (Deledalle *et al.*, 2009) expresses the SAR denoising process as a weighted maximum likelihood estimation problem where the weights are derived in a data-driven way. A problem of this filter is destruction of thin and dark details in the regularized images. Zhong *et al.* (2011) developed a new version of the BNL (Bayesian Non-Local) filter adapted for speckle removal. The new filter incorporates the technique of sigma filter (Lee *et al.*, 2009) to instruct the operation of pixel preselection which is important for detailed preservation. However, the smoothing of homogeneous areas and preserving of edges are still not well balanced in these methods. The BM3D and SAR-BM3D algorithm (Dabov *et al.*, 2007; Parrilli *et al.*, 2012) despeckles SAR images by combining

the concepts of nonlocal filtering and wavelet-domain shrinkage which have a better capacity to preserve relevant details while smoothing homogeneous areas. Lu *et al.* (2013) employ a sparse gradient scheme in a global optimization framework. This method works very well in preserving major edges while smoothening the manageable degree of low-amplitude noise. At present, the BM3D, LMMSE and SAR-BM3D algorithms are well known for their state-of-the-art denoising performance. All these methods denoise the SAR images with patches received after transform domain. However, these algorithms find difficulty in choosing the optimum threshold for finding the patches which is computationally expensive. Since, SAR images assume signal-dependent noise, a novel denoising approach is still an open problem. Also, most of the despeckling algorithms works based on the statistics of pixels and the relationship with their surroundings. However, the adaptive coherence of pixels on different statistical distributions makes the despeckling algorithms hard to set appropriate parameters. In contrast, an alternative way is introduced for despeckling in this study which suppresses speckle by avoiding direct modeling of the speckle. Here, the SAR image is initially segmented by using marker controlled watershed segmentation followed by identifying the coherence pixels at each sub regions to be despeckled. The proposed despeckling method based on coherence vector filter not only denoises the image also preserves the structural characteristics of the image.

This study contributes to speckle filtering techniques on spatial domain. The major improvements identified from spatial filtering from the literature are:

- The method should try to avoid the fixed window size
- The coherence pixels should also be considered and
- The edges and textures should be preserved

MATERIALS AND METHODS

As noted in literature, most of the enhancement techniques used in past research works not only denoise the SAR images but also distorts the background structure such as textures and edges. The filtering method proposed in this paper works in two steps. It starts by dividing the SAR image into number of homogeneous regions and for each region local mean filter is applied to denoise the SAR image. The homogeneous regions are identified by using an improved marker controlled watershed segmentation algorithm and the coherent pixels

are identified with the measure called Intensity Coherence Vector (ICV). These two steps are described in the following text.

To overcome the problem of using fixed window size for the spatial filters, it was introduced to segment the SAR images into homogenous regions by using watershed segmentation. Watershed algorithm has been accepted as an impressive segmentation method due to its multi advantages, like including simplicity, quickness and complete division of the image. The watershed algorithm can produce better segmentation though the image has low contrast and weak boundaries. Grau *et al.* (2004) presented a detailed study of algorithms that make use of the watershed algorithm for image segmentation. The major limitation of the Standard Watershed algorithm is over-segmentation and is sensitive to noise. This problem can be resolved by considering the gradient magnitude image rather than taking the original grayscale image as input to watershed algorithm. However, the variations in gradient magnitude image as well as negative impulse noise observed as a local minimum can result in unexpected additional watershed segments. Further, numerous methods have been proposed to improve the watershed algorithm. Among, the most notable is the usage of region markers where certain desired local minima are selected as markers and then reconstruction is applied to fill the other minima to non-minimum hills. On the other hand, automatic marker selection is a challenging process and in most of the applications, human interaction is required to select appropriate markers. In addition, incorrect markers selection can dramatically affect the final result. The prior knowledge of shapes existed in the image improves the performance of the watershed segmentation as demonstrated in several image segmentation approaches. But still, the major limitation in using prior shape and appearance models is the need to label training set of images and also the set should contain all possible shapes. In this study, initially the SAR image is smoothened by using simple median filter and the edge pixels are used as markers for watershed transformation. Thus, the over-segmentation and sensitive to noise issues of watershed algorithm have been solved.

Watershed segmentation: This study presents classical watershed segmentation algorithm for grayscale images by using spatial distance. The more detailed explanation of the algorithm can be referred in Roerdink and Meijster (2000). For an input image I , the lower slope, $L(a)$ is calculated to find the neighbors for the pixel a which is defined as:

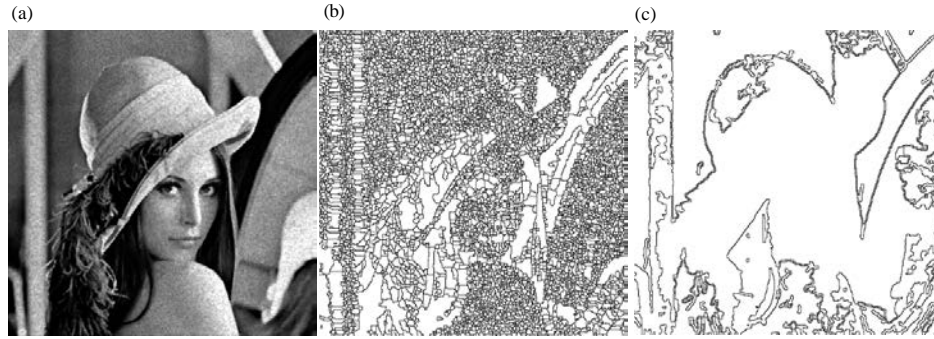


Fig. 1: a) Noisy peppers image; b) Standard watershed segmentation and c) Watershed segmentation with edge markers

$$L(a) = b \in N(a) \cup a \left(\frac{I(a) - I(b)}{d(a, b)} \right)$$

Where:

$N(a)$ = The set of neighbours of pixel a

$d(a, b)$ = The Euclidean distance between a and b

In case of $a = b$, the $L(a)$ value will be forced to be zero. Therefore, the cost for moving from pixel a to b is defined as:

$$\text{cost}(a, b) = \begin{cases} L(a)d(a, b) & \text{if } I(a) > I(b) \\ L(a)d(a, b) & \text{if } I(a) < I(b) \\ 1/2[L(a) + L(b)]d(a, b) & \text{if } I(a) = I(b) \end{cases}$$

If there exists a path $p = (a_0, \dots, a_i)$ from $a_0 = a$ to $a_i = b$, the topographical distance along p between the two pixels a and b is expressed as:

$$T_i^p(a, b) = \sum_{i=1}^{l-1} d(a_i, b_{i+1}) \cos t(a_i, b_{i+1})$$

The T_i^p is the minimum distances among all paths linking the pixels a and b . Similarly, the catchment basin of a local minimum (m) is defined as the set of pixels which have similar topographical distances to m than any other local minimum. At the end, the set of pixels which do not belong to any catchment basin are referred to as the watershed pixels. The major limitation here is the over-segmentation.

Marker controlled watershed segmentation: Meyer and Beucher (1990) and Vincent and Soille (1991) initiated the solutions to over-segmentation problem by applying watershed algorithm with predefined local minimum known as markers. Generally, the edge pixels are used as

markers in most of the segmentation algorithms. Although, this approach is widely used in many segmentation algorithms, the marker selection requires cautious user interaction or prior knowledge of the image structure. The random marker selection algorithms may resolve this problem but there is a possibility of accepting a non-edge pixel as an edge or rejecting an edge pixel as non-edge one. And moreover, these edge detection algorithms may not produce connected edges. The morphological operations can be used to join the disconnected edges. But still, the result highly depends on the selection of wide range of morphological parameters (Hamarneh and Li, 2009). In the proposed method, watershed segmentation is applied with the edge image providing the closed and complete boundaries for the catchment basins. Thus, the over-segmentation has been limited in the proposed watershed method.

Initially, the edges of the SAR image are identified with canny operator (Jain, 1989). The edges are open mostly they do not produce closed boundaries. Here, we applied watershed segmentation with the edge image to make the edges connected and closed. Then, this closed edge boundary is mapped with original grayscale SAR image, each regions enclosed within the edges are extracted from the SAR image, hence the SAR image is segmented with minimum number of regions. Thus, the over-segmentation behavior of watershed algorithm is resolved and the fixed window size based enhancement is avoided. Moreover, the watershed algorithm is sensitive to noise but the problem is ignored here as the proposed algorithm works with the edge map rather than grayscale image. Figure 1 illustrates the improvement in watershed segmentation as it results in minimum number of regions than the classical watershed algorithm. In the next step, Intensity Coherence Vector (ICV) is calculated at each sub-region from watershed algorithm to find the coherent pixels inside the sub region and they are denoised with a simple filtering approach.

Intensity coherence vector: Intuitively, the pixel's intensity coherence is defined as the degree to which pixels of that intensity are members of large similarly-colored regions. These significant regions are referred as coherent regions and it is observed that they are important in characterizing images. The coherence measure ICV classifies pixels as either coherent or incoherent. Coherent pixels are a part of some sizable contiguous region while incoherent pixels are not. A color coherence vector represents this classification for each color in the image. ICV's prevent coherent pixels in one image from matching incoherent pixels in another. This allows fine distinctions that cannot be made with histograms. This property of ICV is used here to identify the local coherence pixels at every sub-region received from improved watershed segmentation algorithm. The following text explains the computation of ICV measure.

Computing ICV's: The first step in computing ICV is similar to the computation of a histogram. Initially, the image is discretized into 'nc' number of distinct intensities to eliminate the small oscillations between neighboring pixels. The next step is to classify the pixels within a given region as either coherent or incoherent. A coherent pixel is a part of a large group of pixels of the same color while an incoherent pixel is not. The pixel group is determined by computing connected components. A connected component C is a maximum set of pixels in such a way that for any two pixels $p, p' \in C$, there is a path in C between p and p' . (Formally, a path in C is a sequence of pixels $p = p_1, p_2, \dots, p_n = p'$ such that each pixel p_i is in C and any two sequential pixels p_i, p_{i+1} are adjacent to each other. Two pixels are considered to be adjacent if one pixel is among the eight closest neighbours of the other. In other words, diagonal neighbors are included). Note that connected components are computed within a given discretized intensity bucket. This effectively segments the sub-region based on the discretized space.

Connected components can be computed in a linear time. When this is complete, each pixel will belong to exactly one connected component. Then, the pixels are classified as either coherent or incoherent depending on the size in pixels of its connected component. A pixel is coherent if the size of its connected component exceeds a fixed value 't'. Otherwise, the pixel is incoherent. For a given discretized intensity range, some of the pixels with that intensity will be coherent and some will be incoherent. Let the number of coherent pixels of the j th discretized color α_j and the number of incoherent pixels β_j and the total number of pixels with that color is $\alpha_j + \beta_j$. For

each color, the pair (α_j, β_j) is computed and it is named as the coherence pair for the intensity. The intensity coherence vector for the image consists of:

$$\langle (\alpha_1, \beta_1), \dots, (\alpha_n, \beta_n) \rangle$$

This is a vector of coherence pairs, one for each discretized intensity value. A numerical example for computing ICVs can be referred by Pass *et al.* (1996).

Coherence despeckling: Once the ICVs are identified for each region, the region is marked with the coherence label. Each label is meant for corresponding coherence pixels. The pixels belonging to one particular label is extracted and their intensity values are received from the original grayscale SAR image to find their mean values. The coherence label region has the minimum of 30% of pixels (Pass *et al.*, 1996). Among the entire pixels in region alone is considered for denoising:

$$\frac{\alpha_j}{n_r} \geq 0.3$$

Where:

α_j = The number of pixels with the coherence label 'j'

n_r = The total number of pixels available in the region

Then the each pixel's intensity value is replaced with the calculated mean value which is defined as:

$$I_i(x, y) = \sum \frac{I_i(x, y)}{nr}, \text{ where } I_i(x, y) \in c_i$$

Where:

c_i = The coherence labels of the region 'r'

$I_i(x, y)$ = The intensity values from the SAR images has the corresponding coherence label c_i

This procedure will be repeated for remaining coherence labels available for the current region. And, the denoising is continued with the next region, till the entire image is denoised. The following algorithm summarizes the proposed despeckling algorithm:

- Step 1: Read as SAR image (If it is a color image than convert it to grayscale)
- Step 2: Find the edge magnitudes of the normalized SAR image by using 'canny' operator
- Step 3: Apply the watershed algorithm on edge map to get closed contours
- Step 4: Discretize the image into 'nc' color bins

- Step 5: Map the edge boundaries with the grayscale image to extract the segmented regions
- Step 6: For each segmented region
 - Find the intensity coherence Vectors and label them
 - For each coherence label
 - Find the local mean value
 - Replace all the pixels corresponding to this coherence label with the mean value
 - Update the pixel values in the noisy SAR image
- Step 7: Output the denoised SAR image

The performance of the proposed filtering approach is compared with other existing denoising approaches and is described in the following study.

RESULTS AND DISCUSSION

In this study, both simulated and real SAR images are used to analyze the performance of the proposed SAR denoising method. Initially, the speckle noise is added to the original images to degrade them. Thus, the original images are treated as the true values and are used as numerical measures to assess the performance. In this experiment, five other methods (i.e., Frost filter, PPB, LMMSE-PCA and BM3D, BNL filter algorithms) are selected to compare with the proposed method. The selection of these methods is based on both availability of the codes and their relevance to this research.

Synthetic images database: A variety of image sources are considered in this experiment including the benchmark test image, Lena, Barbara, boats and lake. A synthetically speckled image is generated by a noise-free image with speckle noise. The L-look amplitude speckled images of size 512×512 disturbed by developed speckle noise is taken for experiments and the performance of algorithms is evaluated by PSNR. The proposed algorithm was implemented in MatLab® environment, the synthetic images are the test image freely available within the MatLab environment.

Real SAR images database: To validate the effectiveness of proposed algorithm, the real SAR images received from four different repositories (ALOS-PALSAR, Sentinel-1, TerraSAR and AirSAR) has been used. The description of each dataset is given below.

PALSAR was one of three instruments on the Advanced Land Observing Satellite-1 (ALOS-1), also known as DAICHI, developed to contribute to the fields of mapping, precise regional land-coverage observation,

Table 1: Summary of real SAR image datasets

Dataset	Band	Type	No. of images
ALOS-PALSAR	L	GeoTiff	25
Sentinel-1	C	GeoTiff	25
TerraSAR	X	GeoTiff	25
AirSAR	L and C	GeoTiff	25

disaster monitoring and resource surveying. ALOS-1 was a mission of the Japan Aerospace Exploration Agency (JAXA) (<https://www.asf.alaska.edu/sar-data/palsar/download-data/>).

Sentinel-1 C-band Synthetic Aperture Radar (SAR) which builds on European Space Agency's and Canada's heritage SAR systems on ERS-1, ERS-2, envisat and Radarsat can be used for natural hazards and disaster risk management, especially in flood situations. Sentinel-1 carries an advanced radar instrument to provide an all-weather, day-and-night supply of imagery of Earth's surface (<https://scihub.esa.int/dhus/>).

TerraSAR-X is a commercial German synthetic aperture radar (SAR) Earth observation satellite which was launched in June 2007. The TerraSAR-X mission is a Public Private Partnership (PPP) between the German Aerospace Centre (DLR) and Europe's leading space company, EADS Astrium GmbH. TerraSAR-X carries a steerable X-Band SAR sensor which provides a highly accurate, high resolution dataset. (<http://terrasar-x-archive.infoterra.de/>).

The Airborne Synthetic Aperture Radar (AIRSAR) was an all-weather imaging tool able to penetrate through clouds and collect data at night. The longer wavelengths could also penetrate into the forest canopy and in extremely dry areas through thin sand cover and dry snow pack. AIRSAR was designed and built by the Jet Propulsion Laboratory (JPL) which also manages the AIRSAR project. AIRSAR served as a NASA radar technology testbed for demonstrating new radar technology and acquiring data for the development of radar processing techniques and applications. (<http://airsar.jpl.nasa.gov>). Table 1 summarizes the datasets used for evaluation.

Performance evaluation: The performance evaluation of filters is an important and basic issue on SAR image despeckling. For synthetic speckle images, the Peak Signal-to-Noise Ratio (PSNR) is used to evaluate the performance of the different methods. And the Signal-to-Clutter Ratio (SCR) is used to evaluate the performance of preservation of strong point targets of the different methods. Also three other different types of quantitative evaluation indicators are used to evaluate the performance of the different filters. For consistent performance, four different noise variation ($\sigma = 10, 20,$

40 and 60) is used. Also, the multi-look images are generated for the synthetic images at four different looks ($L = 1, 2, 4$ and 16). Peak Signal-to-Noise Ratio (PSNR): PSNR (Easley *et al.*, 2008) is decibels (dB) defined as:

$$\text{PSNR} = 20 \log_{10} \frac{255N}{\|f - \hat{f}\|_F}$$

Where:

$\|\cdot\|_F$ = The Frobenius norm, the given image f is of size $N \times N$

\hat{f} = The estimated image

Figure 2 shows the noisy synthetic images and their corresponding denoised images from various despeckling methods. Table 2 quantifies the PSNR measure on every despeckling approach at various speckle level. From the results, it is shown that the proposed method is able to achieve the highest PSNR value than the other existing algorithms. The observation is that the proposed method greatly outperformed LMMSE-PCA and BM3D on most noise levels justifies the proposed denoising model for ASDN. We also observed that the performance of LMMSE-PCA is very sensitive to noise level variation in logarithmic space. As we can see in Table 2, when the



Fig. 2: Continue

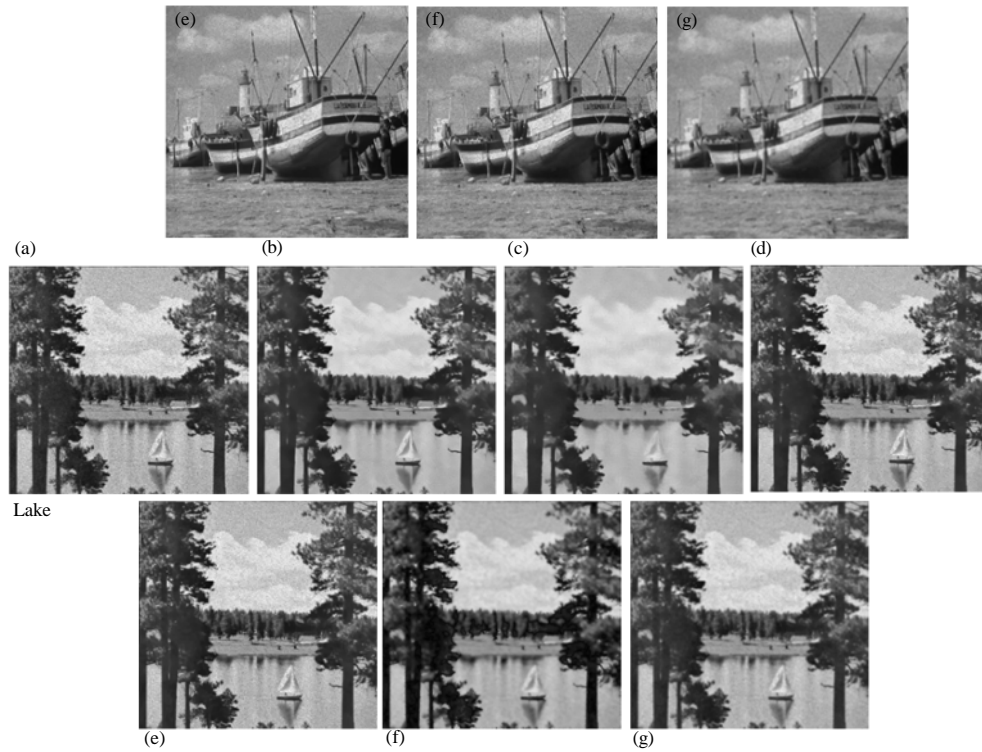


Fig. 2: Denoised output from despeckling methods with synthetic images ($\sigma = 10$, $L = 16$): a) Noisy image; b) ICV Filter; c) PPB; d) BNL; e) BM3D; f) LMMSE and g) Frost filter results

Table 2: Performance analysis of despeckling methods with PSNR measure

Methods	$\sigma = 10$	$\sigma = 20$	$\sigma = 40$	$\sigma = 60$	$L = 1$	$L = 2$	$L = 4$	$L = 16$
Lena								
Noisy image	20.7587	17.1390	11.4867	7.9778	7.3898	11.0270	16.7051	19.6932
ICV filter	27.6268	20.0711	16.6610	11.2797	10.8544	16.5539	19.4281	25.0209
PPB	25.1151	19.5937	16.0637	11.0143	9.3221	16.3793	19.1292	24.6742
BNL	24.8236	19.5841	15.0280	10.5440	8.9056	15.9870	18.9102	24.0532
BM3D	21.9269	19.3041	14.8819	10.2406	8.8051	15.9825	17.5855	23.4370
LMMSE	21.7412	19.1026	14.5995	9.9526	8.5160	13.5168	17.0804	23.2258
Frost filter	21.0583	18.7577	13.6381	8.8053	8.0219	11.9655	16.9041	20.572
Barbara								
Noisy image	25.7887	19.9110	13.2273	7.3121	7.1066	11.5388	17.5223	24.7811
ICV filter	27.9905	25.4334	18.1268	12.8995	11.4685	16.4078	24.5618	27.2124
PPB	27.8136	25.2017	17.0191	12.8456	11.3700	15.4094	24.5255	27.0905
BNL	27.4457	24.9676	15.4558	9.5269	8.9546	14.7728	24.3604	27.0290
BM3D	27.2071	23.9254	14.4024	9.2818	8.7224	13.8627	24.0267	26.7748
LMMSE	26.9410	23.4002	14.3659	8.3967	8.6743	13.6512	23.1624	26.7715
Frost filter	26.7044	22.6765	14.1474	8.2322	7.7550	11.8608	18.7620	24.8376
Peppers								
Noisy image	23.8752	20.8165	14.7640	7.0622	8.1508	11.2913	14.3378	19.0030
ICV filter	27.5116	22.9032	17.4026	14.5931	10.2208	14.1369	17.6345	27.3188
PPB	27.0170	22.6405	17.0358	12.6966	9.3860	13.7977	17.1735	23.3213
BNL	25.7285	21.9789	16.7817	10.1972	8.8878	13.5895	16.5519	22.9350
BM3D	25.0391	21.6603	15.8126	9.8881	8.8658	13.2849	16.3338	21.2592
LMMSE	24.1020	21.2404	14.9977	8.4226	8.4436	12.6139	16.1647	21.1986
Frost filter	23.9733	21.0167	14.8755	8.2988	8.3250	11.9074	15.0863	19.5874
Boats								
Noisy image	25.1094	19.8406	12.9470	7.7345	7.1610	15.2122	20.5740	23.7111
ICV filter	26.9761	24.7120	18.5251	12.9088	13.9471	19.9983	23.1945	26.9547
PPB	26.4919	24.1963	18.1021	12.3379	12.0776	19.8407	23.1872	26.6966
BNL	26.4346	24.1221	14.8668	11.2167	11.9435	18.0256	22.6110	25.1754
BM3D	26.1707	21.4688	14.6793	10.9923	11.8259	17.9991	22.4747	24.8799
LMMSE	25.4933	21.2867	13.8048	9.4299	11.6927	17.8469	20.7467	24.6305
Frost filter	25.1542	20.2983	13.6404	8.2933	10.7575	15.7377	20.7462	24.1430

Table 3: Performance analysis of despeckling methods with SCR measure

Methods	$\sigma = 10$	$\sigma = 20$	$\sigma = 40$	$\sigma = 60$	L = 1	L = 2	L = 4	L = 16
Lena								
Noisy image	3.4991	3.1748	2.6596	2.4265	2.4195	2.5855	2.9135	3.1671
ICV filter	3.7693	3.4900	3.1115	2.6014	2.5757	2.8127	3.1197	3.7660
PPB	3.7658	3.4512	3.0831	2.5663	2.5548	2.7844	3.0869	3.6444
BNL	3.6302	3.3669	3.0612	2.5573	2.5128	2.7411	3.0487	3.3506
BM3D	3.6277	3.3424	2.9463	2.4872	2.4853	2.7251	3.0392	3.2992
LMMSE	3.5954	3.3085	2.9012	2.4693	2.4438	2.6912	2.9558	3.2410
Frost Filter	3.5698	3.1912	2.8066	2.4388	2.4351	2.6303	2.9488	3.1736
Barbara								
Noisy image	3.4028	2.9515	2.6450	2.4236	2.4006	2.7118	3.1700	3.5332
ICV filter	3.7414	3.1390	2.9362	2.6216	2.6784	3.1310	3.5102	3.7622
PPB	3.6931	3.1387	2.9048	2.6109	2.6145	3.0572	3.4071	3.7098
BNL	3.6666	3.1179	2.8788	2.6024	2.5558	3.0122	3.3639	3.6519
BM3D	3.6269	3.0138	2.7634	2.5898	2.4628	2.9165	3.3224	3.6329
LMMSE	3.5536	2.9940	2.7593	2.5682	2.4624	2.8956	3.2892	3.5733
Frost filter	3.4825	2.9851	2.7491	2.4767	2.4566	2.8408	3.1786	3.5383
Peppers								
Noisy image	3.5644	3.1566	2.8407	2.4143	2.5103	2.8761	3.2417	3.4062
ICV filter	3.7616	3.4841	3.1353	2.6177	2.8544	3.2243	3.3563	3.7203
PPB	3.6761	3.4503	3.0962	2.6052	2.7748	3.0754	3.3157	3.6948
BNL	3.6605	3.3998	3.0817	2.5670	2.6843	3.0052	3.2898	3.6696
BM3D	3.6507	3.3836	3.0366	2.5077	2.6705	3.0017	3.2816	3.6672
LMMSE	3.6332	3.1903	3.0175	2.4720	2.5319	2.9070	3.2647	3.5986
Frost filter	3.5780	3.1896	3.0023	2.4390	2.5270	2.8824	3.2424	3.5468
Boats								
Noisy image	3.4093	3.3345	3.0587	2.5204	2.4589	3.0561	3.3334	3.5967
ICV filter	3.7748	3.3755	3.2092	2.9498	2.8368	3.2518	3.5859	3.7837
PPB	3.6751	3.3628	3.1955	2.8967	2.8198	3.2315	3.5417	3.7092
BNL	3.6699	3.3516	3.1824	2.7663	2.7365	3.1365	3.4644	3.6912
BM3D	3.4928	3.3422	3.1000	2.6725	2.6942	3.1364	3.3972	3.6835
LMMSE	3.4400	3.3417	3.0944	2.6268	2.6384	3.1033	3.3578	3.6693
Frost filter	3.4327	3.3396	3.0699	2.6162	2.5506	3.0619	3.3512	3.6385

noise level is low, LMMSE-PCA achieved lower statistics than the proposed method and the same has been depicted in Fig. 2. However, with the increase of noise level, LMMSE-PCA tends to achieve comparable results with our method in terms of PSNR. LMMSE-PCA even achieved higher PSNR on image Lena when the noise level is higher, this is reasonable because LMMSE-PCA was designed for AWGN. In case noise level is high, the speckle noise subject to logarithmic operation which is very close to the Gaussian white noise. Therefore, the method can achieve good results. However, when the noise level is small, speckle noise begins to deviate from Gaussian distribution and its mean value is no more zero. This discrepancy between the empirical data and the model assumption may reduce the efficiency of LPG-PCA. Figure 2 illustrates the sample outputs from the proposed despeckling and five other existing methods with synthetic images at noise variance 10 with 16 multiple looks, images by the proposed method have little artifacts but plenty of image details.

Signal-to-Clutter Ratio (SCR): Clutter is a term used to describe any object that may generate unwanted radar returns and which may interfere with normal radar

operations. Clutter echoes are random and have thermal noise-like characteristics because the individual clutter components (scatterers) have random phases and amplitudes. In many cases, the clutter signal level is much higher than the receiver noise level. Thus, the radar's ability to detect targets embedded in high clutter background depends on the Signal-to-Clutter Ratio (SCR) rather than the SNR. Here, the edge pixels are considered as clutters (target pixels). SCR can be used to evaluate the performance of preserving strong point targets in as SAR image. SCR is decibels (dB) defined as (Hou *et al.*, 2012):

$$SCR = 10 \log_{10} \frac{\sum_i \sum_j |\hat{s}(i, j)|}{N \sigma_c}$$

Where:

$\hat{s}(i, j)$ = The point target pixel value

N = The total number of point target pixels

σ_c = The clutter standard deviation

A large SCR value corresponds to better speckle suppression. Table 3 depicts the SCR values received from despeckling methods. Again, the proposed method outperforms other methods by attaining the highest SCR

Table 4: Performance analysis of despeckling methods with β measure

Methods	$\sigma = 10$	$\sigma = 20$	$\sigma = 40$	$\sigma = 60$	L = 1	L = 2	L = 4	L = 16
Lena								
Noisy image	0.8906	0.7787	0.6685	0.6005	0.6405	0.7162	0.7962	0.9147
ICV filter	0.9595	0.8555	0.7778	0.6683	0.7048	0.7869	0.9082	0.9799
PPB	0.9569	0.8403	0.7556	0.6658	0.6820	0.7695	0.8998	0.9724
BNL	0.9479	0.8168	0.7455	0.6475	0.6781	0.7562	0.8877	0.9539
BM3D	0.9185	0.8058	0.7074	0.6459	0.6741	0.7531	0.8864	0.9253
LMMSE	0.9171	0.7882	0.6910	0.6361	0.6741	0.7199	0.8455	0.9214
Frost filter	0.8998	0.7820	0.6785	0.6164	0.6482	0.7176	0.8119	0.9195
Barbara								
Noisy image	0.8369	0.7524	0.6673	0.6055	0.6126	0.7662	0.8703	0.9444
ICV filter	0.9709	0.8253	0.7486	0.6614	0.7438	0.8675	0.9410	0.9699
PPB	0.9283	0.8099	0.7291	0.6527	0.7353	0.8376	0.9399	0.9596
BNL	0.8699	0.7931	0.7230	0.6517	0.7222	0.8309	0.9292	0.9566
BM3D	0.8539	0.7913	0.6773	0.6344	0.7069	0.8259	0.9256	0.9561
LMMSE	0.8475	0.7859	0.6754	0.6317	0.6786	0.8135	0.9232	0.9551
Frost filter	0.8472	0.7634	0.6690	0.6182	0.6609	0.8062	0.8731	0.9542
Peppers								
Noisy image	0.9236	0.8237	0.7038	0.6201	0.6013	0.7092	0.7937	0.8914
ICV filter	0.9653	0.9138	0.8170	0.6973	0.7058	0.7754	0.8750	0.9772
PPB	0.9621	0.9088	0.8111	0.6932	0.7051	0.7492	0.8602	0.9753
BNL	0.9418	0.9085	0.7936	0.6926	0.7027	0.7245	0.8540	0.9373
BM3D	0.9375	0.8679	0.7927	0.6860	0.6919	0.7179	0.8519	0.9229
LMMSE	0.9353	0.8413	0.7294	0.6858	0.6796	0.7135	0.8509	0.9125
Frost filter	0.9347	0.8367	0.7262	0.6741	0.6504	0.7134	0.8460	0.9078
Boats								
Noisy image	0.9045	0.8232	0.7259	0.6104	0.6075	0.6574	0.7572	0.8881
ICV filter	0.9713	0.8988	0.8223	0.7249	0.6506	0.7445	0.8864	0.9665
PPB	0.9673	0.8813	0.8140	0.7240	0.6486	0.7261	0.8853	0.9452
BNL	0.9440	0.8569	0.8006	0.7195	0.6412	0.7189	0.8713	0.9371
BM3D	0.9351	0.8508	0.7551	0.6668	0.6323	0.6964	0.8095	0.9336
LMMSE	0.9334	0.8339	0.7510	0.6508	0.6187	0.6909	0.7997	0.9177
Frost filter	0.9212	0.8234	0.7494	0.6231	0.6168	0.6902	0.7943	0.9176

value than others for all the synthetic images. Two more measures are used to analyze the edge preservation quality of the proposed algorithm. The first parameter β is used to evaluate the performance of edge preservation. It is originally defined as (Sattar *et al.*, 1997):

$$\beta = \frac{\Gamma(\Delta S - \mu(\Delta S), \Delta \hat{S} - \mu(\Delta \hat{S}))}{\sqrt{\Gamma(\Delta S - \mu(\Delta S), \Delta S - \mu(\Delta S)) \Gamma(\Delta \hat{S} - \mu(\Delta \hat{S}), \Delta \hat{S} - \mu(\Delta \hat{S}))}}$$

where, ΔS and $\Delta \hat{S}$ are the highpass-filtered versions of the original image S and the denoised image \hat{S} , respectively obtained with a window size of 3×3 standard approximation of the Laplacian operator. The over-line operator represents the mean value $\Gamma(S_1, S_2)$ and $\sum_{i=1}^n s_{i1} \cdot s_{i2}$. The correlation measure β should be close to unity for an optimal effect of edge preservation. Table 4 shows the values of the β measure calculated for each denoising methods. The greater value of the proposed method states that this algorithm can preserve the edges better than any other methods.

Edge-Preserved Index (EPI) is another effective measure to evaluate the edge preservation for real SAR

image which is stable for different types of edge images and is only affected by the speckle level. The EPI can be represented as (Waske *et al.*, 2007):

$$EPI = \frac{\sum_{i=1}^m |I_{D1}(i) - I_{D2}(i)|}{\sum_{i=1}^m |I_{O1}(i) - I_{O2}(i)|}$$

Where:

m = The pixel number of the selected area
 $I_{D1}(i)$ and $I_{D2}(i)$ = The adjacent pixel values of the despeckled image along horizontal direction

Similarly, $I_{O1}(i)$ and $I_{O2}(i)$ represent the adjacent pixel values of the original image. The ideal value of EPI is equal to one. The EPI is closer to one which means better ability of edge preservation. Table 5 presents the EPI values of each denoising methods. The closer value to one for the proposed method states that this algorithm can preserve the edges better than any other methods.

The average performance of the proposed despeckling method on synthetic images is analyzed with the noise variance 10 and 20, number of looks

Table 5: Performance analysis of despeckling methods with EPI measure

Methods	$\sigma = 10$	$\sigma = 20$	$\sigma = 40$	$\sigma = 60$	L = 1	L = 2	L = 4	L = 16
Lena								
Noisy image	0.7561	0.6818	0.6122	0.4833	0.4517	0.5189	0.5908	0.6532
ICV filter	0.8305	0.7479	0.6807	0.5967	0.5021	0.5826	0.6518	0.8332
PPB	0.8072	0.7386	0.6729	0.5769	0.4792	0.5816	0.6514	0.8087
BNL	0.8052	0.7127	0.6590	0.5516	0.4763	0.5728	0.6298	0.7937
BM3D	0.7967	0.7098	0.6589	0.5321	0.4747	0.5662	0.6254	0.7862
LMMSE	0.7900	0.6864	0.6569	0.5222	0.4708	0.5660	0.6159	0.7817
Frost filter	0.7783	0.6833	0.6324	0.5174	0.4661	0.5399	0.6034	0.7146
Barbara								
Noisy image	0.7126	0.6050	0.5417	0.4501	0.4741	0.5899	0.6347	0.7241
ICV filter	0.8454	0.7057	0.5952	0.5360	0.5836	0.6241	0.7237	0.8363
PPB	0.8385	0.7014	0.5799	0.5029	0.5822	0.6164	0.7165	0.7724
BNL	0.7801	0.6898	0.5789	0.4957	0.5546	0.6121	0.7125	0.7635
BM3D	0.7498	0.6676	0.5733	0.4874	0.5105	0.6085	0.7040	0.7524
LMMSE	0.7310	0.6560	0.5548	0.4859	0.4982	0.5998	0.6511	0.7426
Frost filter	0.7230	0.6308	0.5447	0.4564	0.4946	0.5949	0.6414	0.7393
Peppers								
Noisy image	0.7802	0.5871	0.5054	0.4535	0.4549	0.5516	0.6655	0.7584
ICV filter	0.8486	0.7798	0.5824	0.5042	0.5481	0.6592	0.7481	0.8401
PPB	0.8413	0.6856	0.5451	0.4948	0.5001	0.6413	0.7453	0.8220
BNL	0.8401	0.6850	0.5331	0.4828	0.4901	0.6386	0.7348	0.8148
BM3D	0.8265	0.6489	0.5265	0.4542	0.4714	0.5728	0.7345	0.8082
LMMSE	0.8181	0.6334	0.5181	0.4538	0.4624	0.5601	0.7050	0.8008
Frost filter	0.8069	0.6134	0.5164	0.4537	0.4579	0.5533	0.7035	0.7654
Boats								
Noisy image	0.7574	0.7107	0.5932	0.4817	0.4726	0.5448	0.5938	0.6653
ICV filter	0.8245	0.7458	0.7098	0.5787	0.5354	0.5827	0.6568	0.8188
PPB	0.8137	0.7333	0.7019	0.5264	0.4931	0.5819	0.6460	0.7834
BNL	0.8060	0.7323	0.7004	0.5252	0.4914	0.5719	0.6333	0.7577
BM3D	0.7945	0.7311	0.6902	0.4969	0.4887	0.5678	0.6145	0.7533
LMMSE	0.7821	0.7230	0.6792	0.4944	0.4872	0.5607	0.6078	0.7067
Frost filter	0.7637	0.7202	0.6028	0.4941	0.4855	0.5488	0.5944	0.6906

Table 6: ANOVA statistics for the performance of ICV filter

Performance measure	F statistics	p-values
PSNR	48.8709	2.90e-19
SCR	51.5377	6.18e-20
β -value	34.8776	2.47e-15
EPI	56.5709	3.78e-21

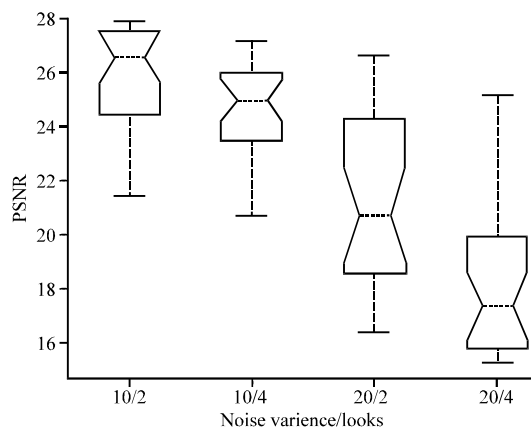


Fig. 3: Denoising performance of ICV filter on PSNR measure

2 and 4. The ICV filter based denoising is applied on synthetic images for 20 times at different combinations

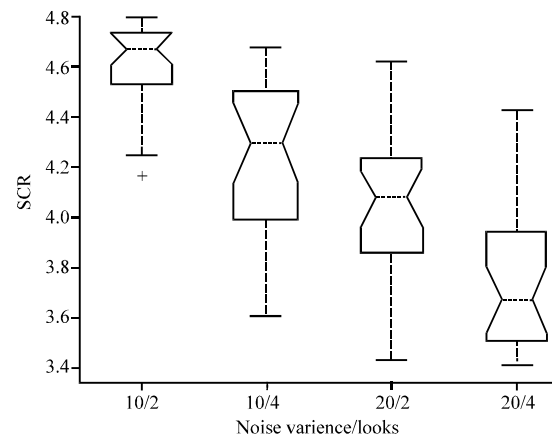


Fig. 4: Denoising performance of ICV filter on SCR measure

of noise variance and looks. The ANOVA test is performed to analyze the significance of noise variance and the number of looks, Fig. 3-6 depicts the performance comparisons.

The summarized ANOVA statistics is depicted in Table 6. The higher F value and the lower p value represents that the noise variance and the number

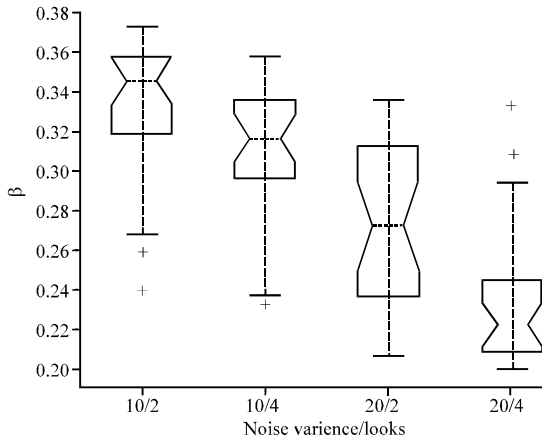


Fig. 5: Denoising performance of ICV filter on β measure

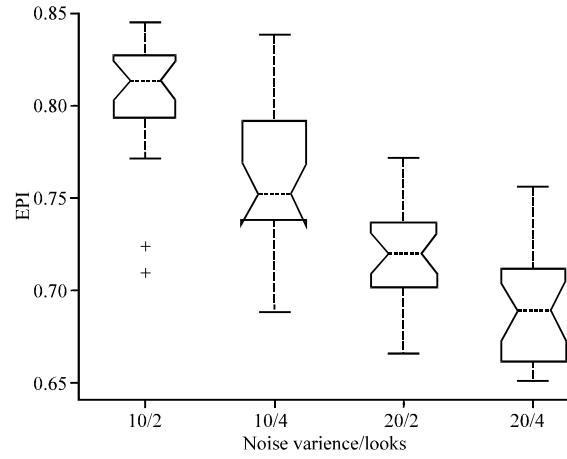


Fig. 6: Denoising performance of ICV filter on EPI measure

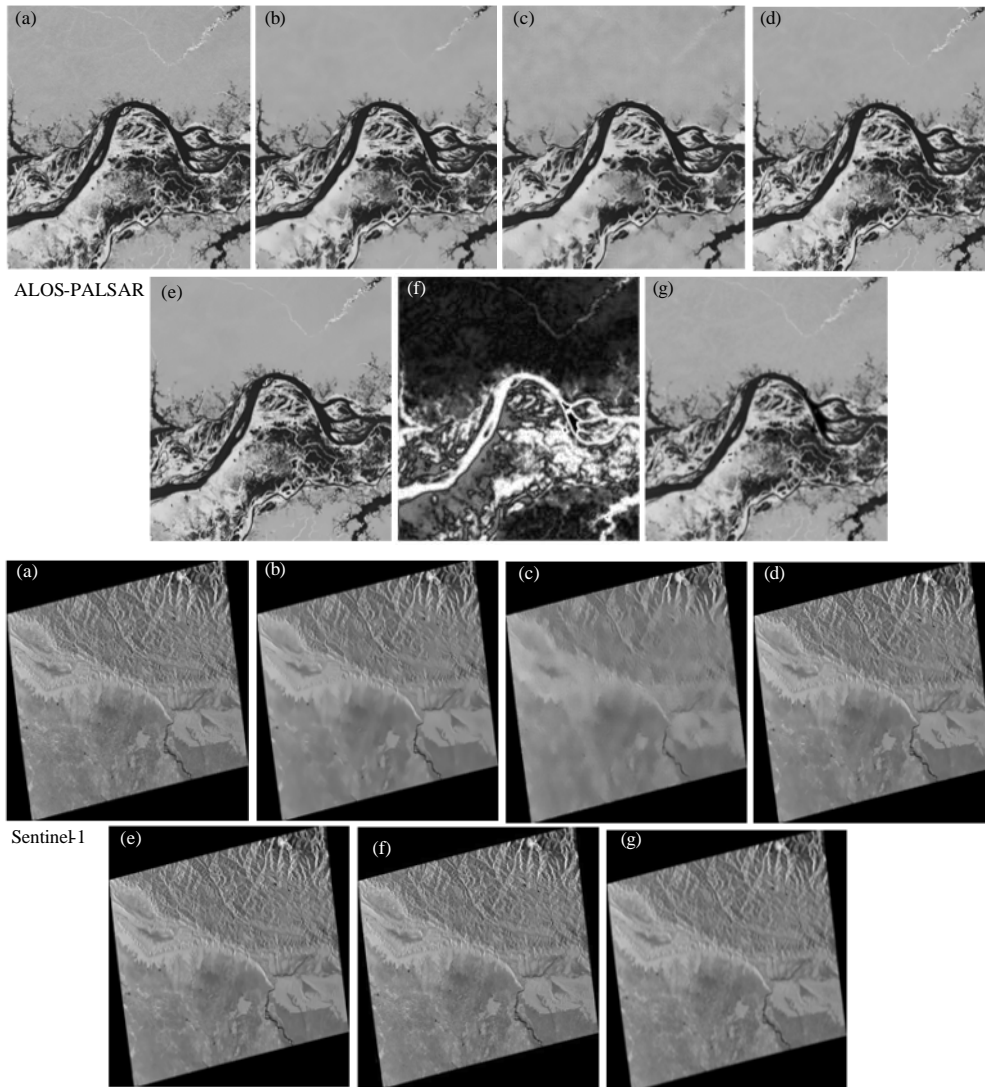


Fig. 7: Continue

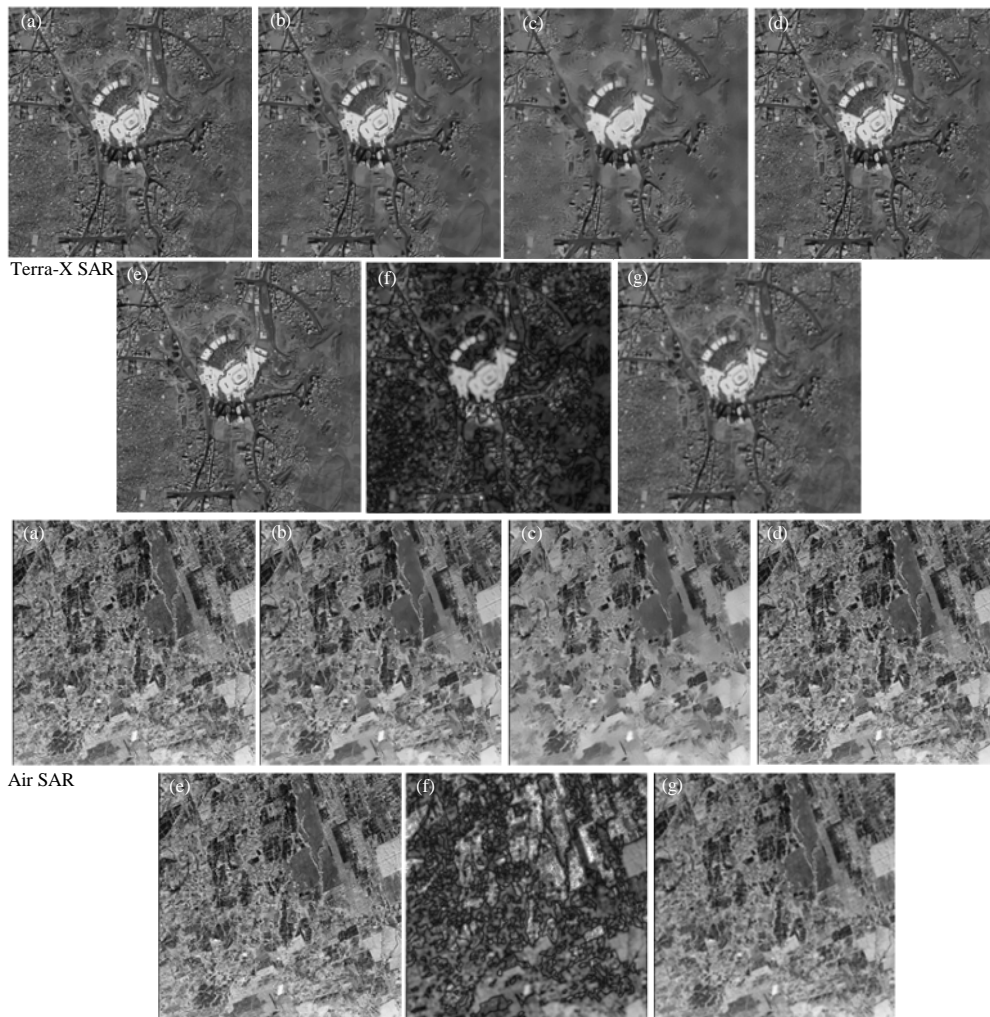


Fig. 7: Denoised output from despeckling methods with real SAR images ($L = 4$): a) Noisy image; b) ICV filter; c) PPB; d) BNL; e) BM3D; f) LMMSE and g) Frost filter results

of looks cause significant changes on denoising performances, for almost all the parameters. Figure 7 illustrates the sample output of proposed and existing despeckling with real SAR image at the maximum of 4 different looks.

CONCLUSION

In this study, an SAR image despeckling scheme is proposed based on coherence structure based segmentation with local mean filtering. Initially, watershed algorithm is applied with the edge image to receive the homogeneous regions from the SAR image for each region. The coherent pixels identified by using Intensity Coherence Vector (ICV) measure are applied with local mean filtering. And these patches are merged together to form complete denoised image. Hence, the proposed approach does not make use of any fixed window size. It

considers the coherence pixels for denoising through ICV and edge marker based segmentation as well as it preserves the boundaries. The proposed denoising scheme is tested on both synthetic and real SAR images and is compared with several other state-of-the-art methods.

The results demonstrate that the proposed method is comparatively better than referenced methods both in terms of image detail preservation and speckle noise reduction.

REFERENCES

- Achim, A., P. Tsakalides and A. Bezerianos, 2003. SAR image denoising via Bayesian wavelet shrinkage based on heavy-tailed modeling. *Geosci. Remote Sens. IEEE. Trans.*, 41: 1773-1784.

- Argenti, F. and L. Alparone, 2002. Speckle removal from SAR images in the undecimated wavelet domain. *Geosci. Remote Sens. IEEE. Trans.*, 40: 2363-2374.
- Baraldi, A. and F. Parmiggiani, 1995. A refined gamma MAP SAR speckle filter with improved geometrical adaptivity. *Geosci. Remote Sens. IEEE. Trans.*, 33: 1245-1257.
- Bianchi, T., F. Argenti and L. Alparone, 2008. Segmentation-based MAP despeckling of SAR images in the undecimated wavelet domain. *Geosci. Remote Sens. IEEE. Trans.*, 46: 2728-2742.
- Buades, A., B. Coll and J.M. Morel, 2005. A review of image denoising algorithms, with a new one. *Multiscale Model. Simul.*, 4: 490-530.
- Chen, J., J. Gao, Y. Zhu, W. Yang and P. Wang, 2012. A novel image formation algorithm for high-resolution wide-swath spaceborne SAR using compressed sensing on azimuth displacement phase center antenna. *Prog. Electromagnet. Res.*, 125: 527-543.
- Cheng, J., G. Gao, W. Ding, X. Ku and J. Sun, 2013. An improved scheme for parameter estimation of G° distribution model in high-resolution SAR images. *Prog. Electromagnet. Res.*, 134: 23-46.
- Dabov, K., A. Foi, V. Katkovnik and K. Egiazarian, 2007. Image denoising by sparse 3-D transform-domain collaborative filtering. *IEEE Trans. Image Proces.*, 16: 2080-2095.
- Dai, M., C. Peng, A.K. Chan and D. Loguinov, 2004. Bayesian wavelet shrinkage with edge detection for SAR image despeckling. *Geosci. Remote Sens. IEEE. Trans.*, 42: 1642-1648.
- Deledalle, C.A., L. Denis and F. Tupin, 2009. Iterative weighted maximum likelihood denoising with probabilistic patch-based weights. *Image Proc. IEEE. Trans.*, 18: 2661-2672.
- Easley, G., D. Labate and W.Q. Lim, 2008. Sparse directional image representations using the discrete shearlet transform. *Applied Comput. Harmonic Anal.*, 25: 25-46.
- Foucher, S., G.B. Benie and J.M. Boucher, 2001. Multiscale MAP filtering of SAR images. *IEEE Trans. Image Process.*, 10: 49-60.
- Frost, V.S., J.A. Stiles K.S. Shanmugan and J.C. Holtzman, 1982. A model for radar images and its application to adaptive digital filtering of multiplicative noise. *IEEE Trans. Pattern Anal. Mach. Intel.*, 4: 157-166.
- Gleich, D. and M. Datcu, 2007. Wavelet-based despeckling of SAR images using Gauss-Markov random fields. *Geosci. Remote Sens. IEEE. Trans.*, 45: 4127-4143.
- Grau, V., A.U.J. Mewes, M. Alcaniz, R. Kikinis and S.K. Warfield, 2004. Improved watershed transform for medical image segmentation using prior information. *Trans. Med. Imag.*, 23: 447-458.
- Hamarneh, G. and X. Li, 2009. Watershed segmentation using prior shape and appearance knowledge. *Image Vision Comput.*, 27: 59-68.
- Hou, B., X. Zhang, X. Bu and H. Feng, 2012. SAR image despeckling based on nonsubsampling shearlet transform. *Sel. Top. Appl. Earth Obs. Remote Sens. IEEE. J.*, 5: 809-823.
- Iqbal, M., J. Chen, W. Yang, P. Wang and B. Sun, 2013. SAR image despeckling by selective 3D filtering of multiple compressive reconstructed images. *Prog. Electromagnet. Res.*, 134: 209-226.
- Jain, A.K., 1989. *Fundamentals of Digital Image Processing*. Prentice Hall, Englewood Cliffs, NJ, USA., ISBN-10: 0133361659.
- Kuan, D.T., A.A. Sawchuk, T.C. Strand and P. Chavel, 1985. Adaptive noise smoothing filter for images with signal-dependent noise. *Pattern Anal. Mach. Intel. IEEE. Trans.*, 2: 165-177.
- Lee, J.S., 1980. Digital image enhancement and noise filtering by use of local statistics. *IEEE Trans. Pattern Anal. Mach. Intel.*, 2: 165-168.
- Lee, J.S., 1981. Refined filtering of image noise using local statistics. *Comput. Graph. Image Proces.*, 15: 380-389.
- Lee, J.S., 1986. Speckle suppression and analysis for synthetic aperture radar images. *Opt. Eng.*, 25: 255636-255636.
- Lee, J.S., J.H. Wen, T.L. Ainsworth, K.S. Chen and A.J. Chen, 2009. Improved sigma filter for speckle filtering of SAR imagery. *Geosci. Remote Sens. IEEE. Trans.*, 47: 202-213.
- Lee, J.S., L. Jurkevich, P. Dewaele, P. Wambacq and A. Oosterlinck, 1994. Speckle filtering of synthetic aperture radar images: A review. *Remote Sens. Rev.*, 8: 313-340.
- Li, J., S. Zhang and J. Chang, 2012. Applications of compressed sensing for multiple transmitters multiple azimuth beams SAR imaging. *Prog. Electromagnet. Res.*, 127: 259-275.
- Liu, G., W. Yang, G.S. Xia and M. Liao, 2013. Structure preserving SAR image despeckling via L0-minimization. *Prog. Electromagnet. Res.*, 141: 347-367.
- Lopez, A., R. Touzi and E. Nezry, 1990. Adaptive speckle filters and scene heterogeneity. *IEEE Trans. Geosci. Remote Sensing*, 28: 992-1000.
- Lu, Y., Q. Gao, D. Sun and D. Zhang, 2013. SAR image despeckling with adaptive multiscale products based on directionlet transform. *Math. Prob. Eng.*, 2013: 1-9.
- Meyer, F. and S. Beucher, 1990. Morphological segmentation. *J. Visual Commun. Image Represent.*, 1: 21-46.

- Molina, D.E., D. Gleich and M. Datcu, 2012. Evaluation of Bayesian despeckling and texture extraction methods based on Gauss-Markov and auto-binomial Gibbs random fields: Application to TerraSAR-X data. *Geosci. Remote Sens. IEEE. Trans.*, 50: 2001-2025.
- Muresan, D.D. and T.W. Parks, 2003. Adaptive principal components and image denoising. *ICIP.*, 1: 101-104.
- Parrilli, S., M. Poderico, C.V. Angelino and L. Verdoliva, 2012. A nonlocal SAR image denoising algorithm based on LLMMSE wavelet shrinkage. *Geosci. Remote Sens. IEEE. Trans.*, 50: 606-616.
- Pass, G., R. Zabih and J. Miller, 1996. Comparing images using color Coherence vectors. *Proceedings of the 4th International ACM Multimedia Conference*, November 18-22, 1996, Boston, pp: 65-74.
- Pizurica, A., W. Philips, I. Lemahieu and M. Acheroi, 2003. A versatile wavelet domain noise filtration technique for medical imaging. *IEEE Trans. Med. Imag.*, 22: 323-331.
- Ranjani, J.J. and S.J. Thiruvengadam, 2010. Dual-tree complex wavelet transform based SAR despeckling using interscale dependence. *Geosci. Remote Sens. IEEE. Trans.*, 48: 2723-2731.
- Ren, S., W. Chang, T. Jin and Z. Wang, 2011. Automated SAR reference image preparation for navigation. *Prog. Electromagnet. Res.*, 121: 535-555.
- Roerdink, J.B.T.M. and A. Meijster, 2000. The watershed transform: Definitions, algorithms and parallelization strategies. *Fundam. Inf.*, 41: 187-228.
- Sattar, F., L. Floreby, G. Salomonsson and B. Lovstrom, 1997. Image enhancement based on a nonlinear multiscale method. *IEEE Trans. Image Proc.*, 6: 888-895.
- Sveinsson, J.R. and J.A. Benediktsson, 2003. Almost translation invariant wavelet transformations for speckle reduction of SAR images. *Geosci. Remote Sens. IEEE. Trans.*, 41: 2404-2408.
- Vincent, L. and P. Soille, 1991. Watersheds in digital spaces: An efficient algorithm based on immersion simulations. *IEEE Trans. Pattern Anal. Mach. Intell.*, 13: 583-598.
- Waske, B., M. Braun and G. Menz, 2007. A segment-based speckle filter using multisensoral remote sensing imagery. *Geosci. Remote Sens. Lett. IEEE.*, 4: 231-235.
- Xie, H., L.E. Pierce and F.T. Ulaby, 2002. SAR speckle reduction using wavelet denoising and markov random field modeling. *Geosci. Remote Sens. IEEE. Trans.*, 40: 2196-2212.
- Xu, L., J. Li, Y. Shu and J. Peng, 2014. SAR image denoising via clustering-based principal component analysis. *Geosci. Remote Sens. IEEE. Trans.*, 52: 6858-6869.
- Yu, Y. and T.S. Acton, 2002. Speckle reducing anisotropic diffusion. *IEEE Trans. Image Process.*, 11: 1260-1270.
- Zhang, L., W. Dong, D. Zhang and G. Shi, 2010. Two-stage image denoising by principal component analysis with local pixel grouping. *Pattern Recognit.*, 43: 1531-1549.
- Zhong, H., Y. Li and L.C. Jiao, 2011. SAR image despeckling using bayesian nonlocal means filter with sigma preselection. *Geosci. Remote Sens. Lett. IEEE.*, 8: 809-813.
- Zhou, Z.F. and P.L. Shui, 2007. Contourlet-based image denoising algorithm using directional windows. *Electron. Lett.*, 43: 92-93.